	Number of Channels	Average cell speed at 10psi (m/s)
Original Design	45	0.1
New Design (iS model)	75	0.35

Table S1. A comparison of between the originally reported device designs and the latest generation described herein. Average cell speeds are estimated at the constriction point of a 10-6 device. Because throughput at a given pressure is dependent on the number of parallel channels and the average cell speed, the new design yields an estimated 6x higher throughput at a given operating pressure.

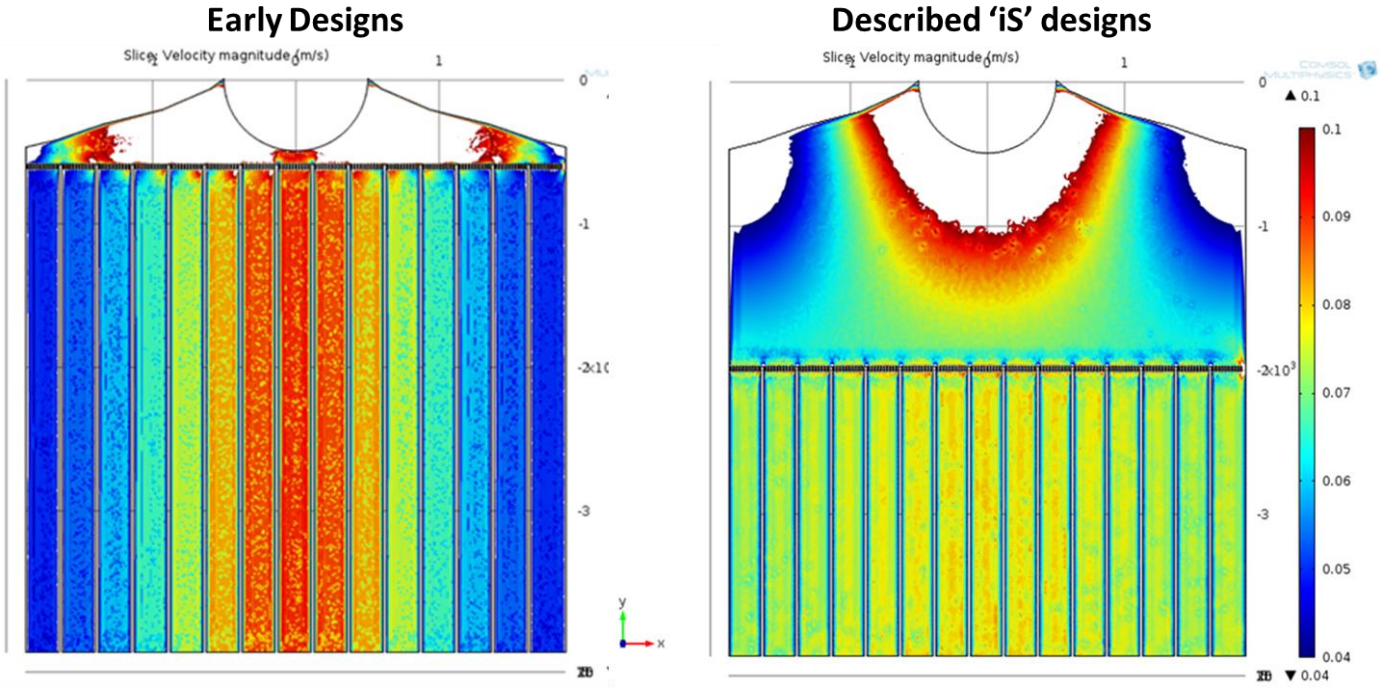

Figure S1. 3-D COMSOL multiphysics simulations of fluid flow in different design schemes. The original designs were found to have a 2-3x variability in flow speed across cell channels. This effect could potentially be caused by the inability of the flow profile to fully develop in the entrance region before it is split into multiple channels. The newer 'iS' design provides a longer entry region for the flow profile to fully form before it is split into smaller channels. In this design, flow speeds across channels were within 20-30% of each other.

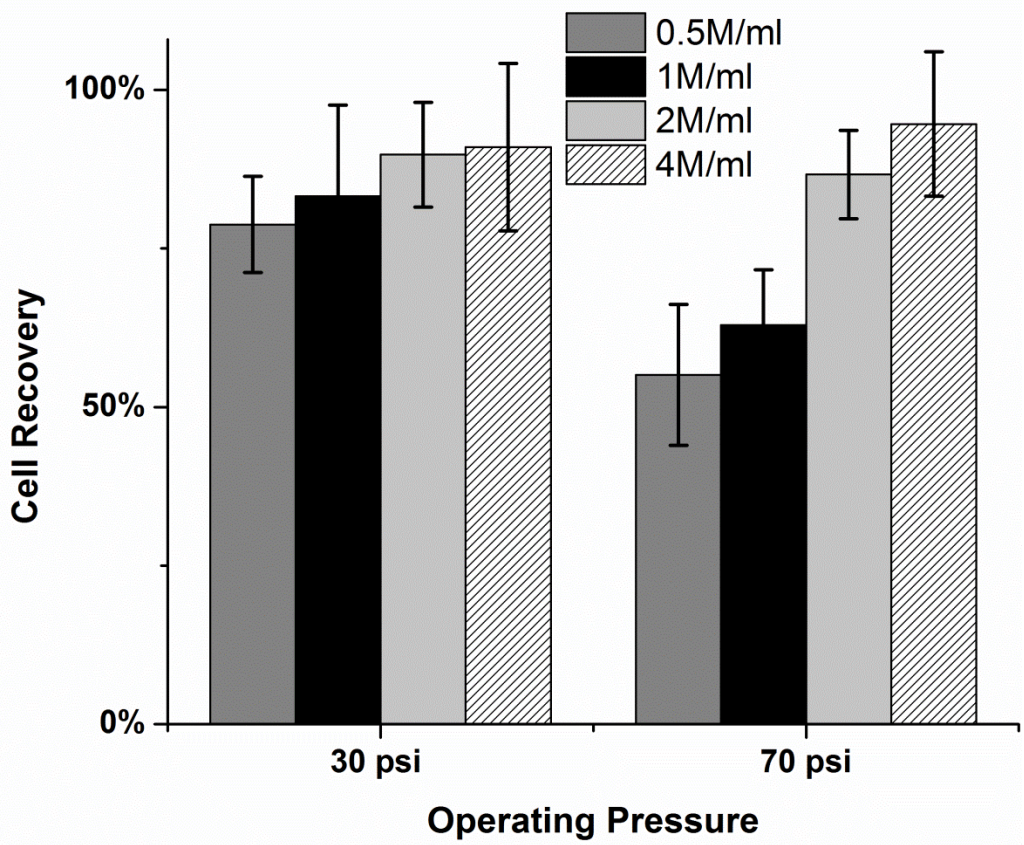

Figure S2. Average cell recovery rates from a 10-6 device. Recovery rates were measured at 4 different suspension concentrations as indicated. Error bars represent two standard deviation across three different tested devices. The experiments described in this article were run at a cell concentrations of 2-10x10^6 cells/ml.

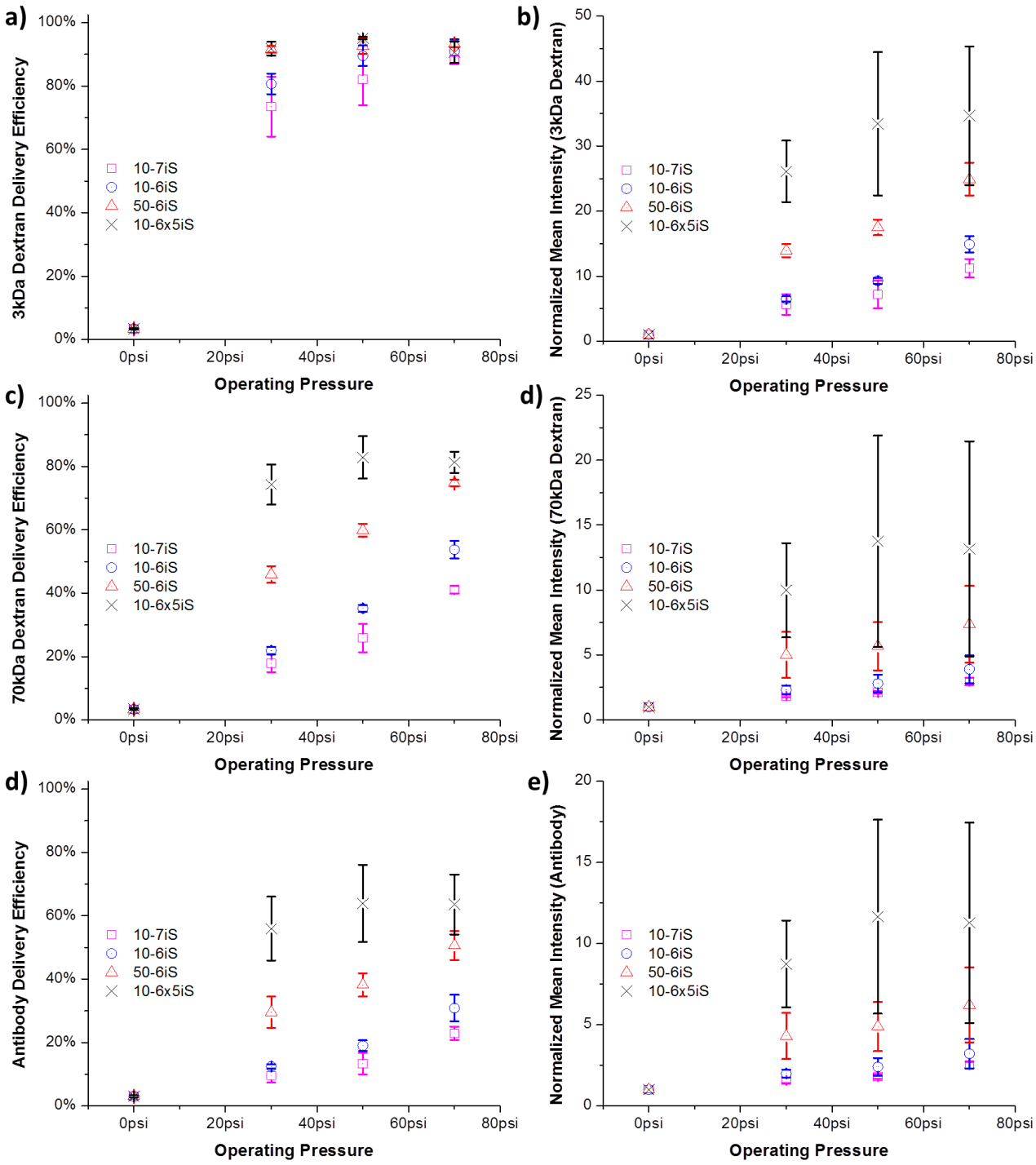

Figure S3. Delivery Efficiency and intensity across four different device designs. Delivery efficiency and normalized delivery intensity of HeLa cells treated by 10-7, 10-6, 50-6, and 10-6x5 devices. Experiments were conducted in PBS and cells were treated in the presence of cascade blue conjugated 3kDa dextran, fluorescein conjugated 70kDa dextran, and APC conjugated IgG1 isotype controls. Results were measured by flow cytometry and viability was measured by propidium iodide staining. Error bars represent 2 standard deviations among triplicates.

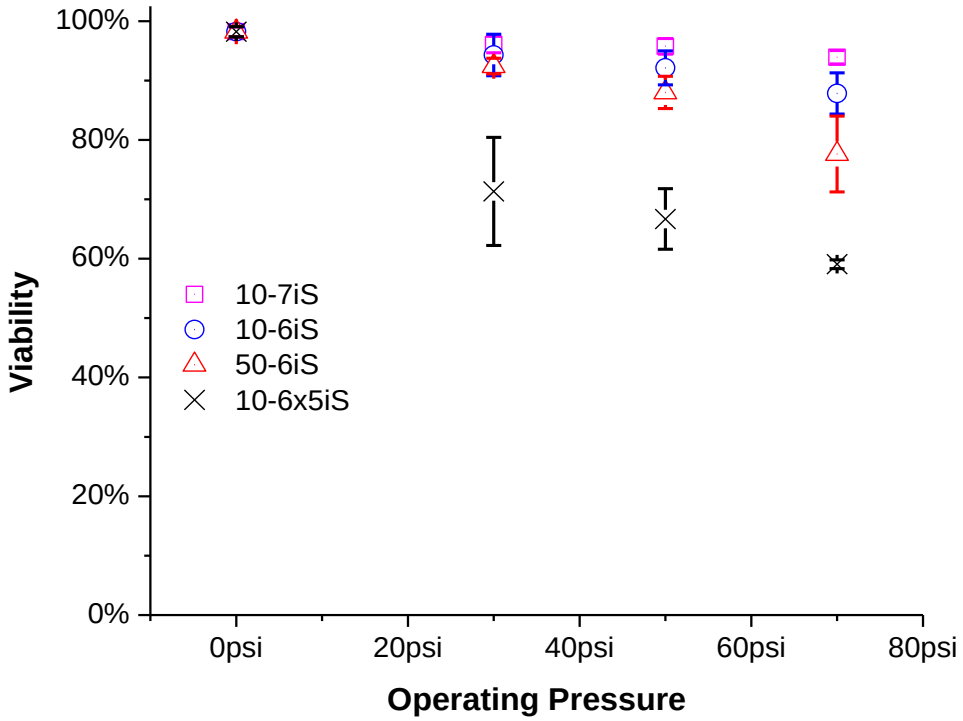

Figure S4. Cell viability across four different device designs. These viability data correspond to the experiments shown in Fig. 2 and Fig. S3. Results were measured by flow cytometry and viability was measured by propidium iodide staining. Error bars represent 2 standard deviations among triplicates.

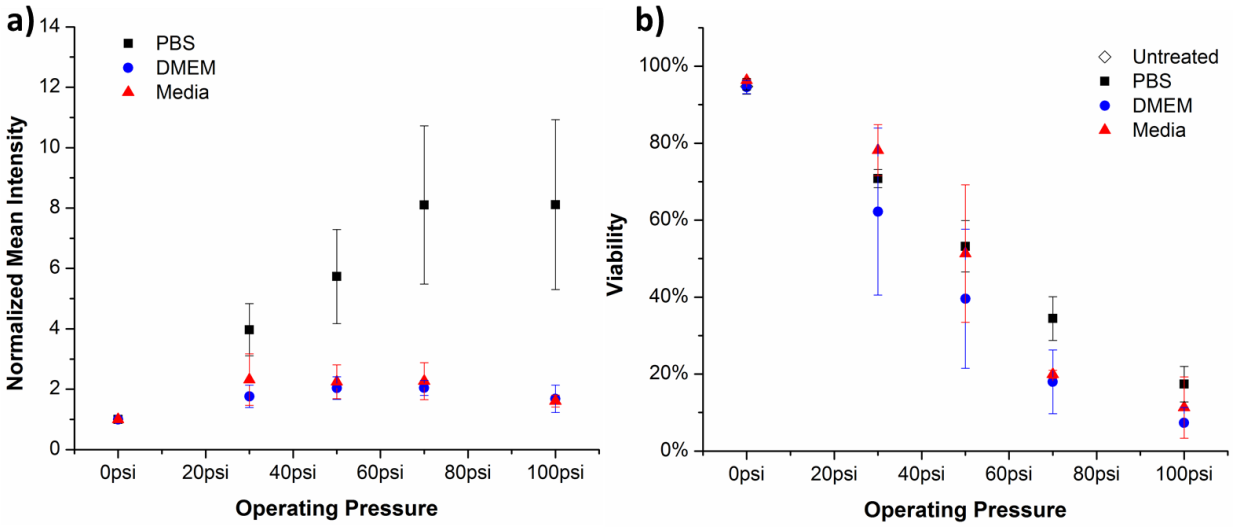

Figure S5. A comparison across flow buffers. a) Normalized delivery intensity of HeLa cells treated in PBS, DMEM, and full culture media using a 50-6 device. **b)** Corresponding viability data as measured by propidium iodide staining. Mean intensity of cascade blue conjugated 3kDa dextran was measured by flow cytometry and normalized against the control to account for background effects (e.g. endocytosis and surface binding). Error bars represent 2 standard deviations among triplicates.

Note that most membrane recovery studies in this work were conducted using the relatively harsh 50-6 device in the hope of providing significant contrast between tested parameters. When similar experiments were conducted using other device designs, similar buffer and temperature dependence behavior was observed.

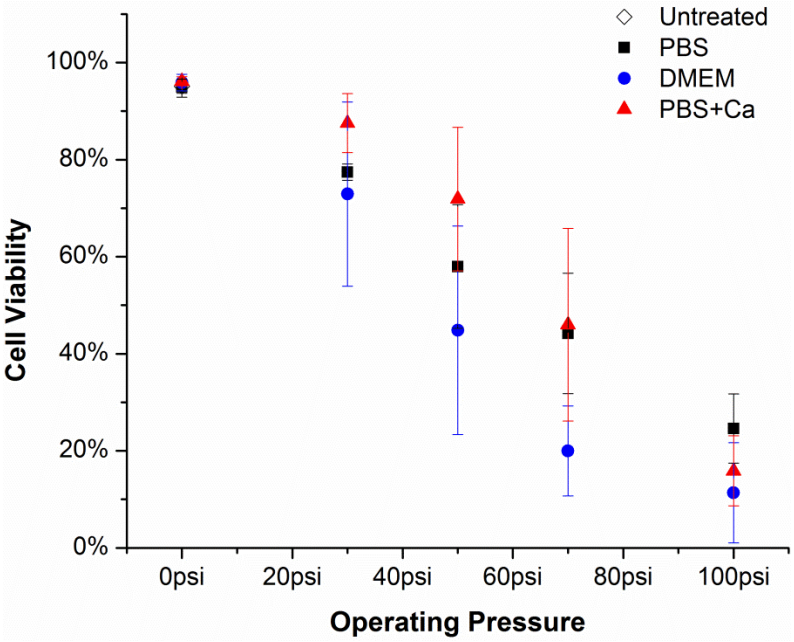

Figure S6. Viability data for HeLa cells treated in PBS, DMEM, and PBS+Ca buffers. These viability data correspond to the experiments shown in Fig. 3b. Results were measured by flow cytometry and viability was measured by propidium iodide staining. Error bars represent 2 standard deviations among triplicates.

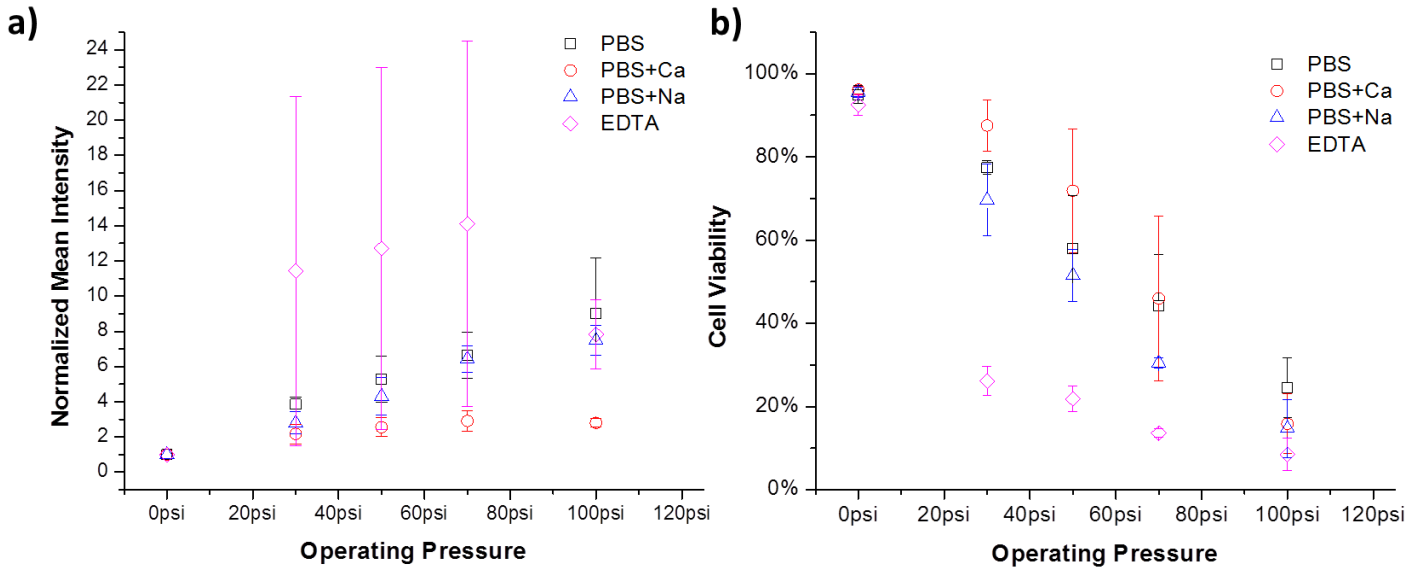

Figure S7. A comparison across ions and chelating agents. a) Normalized delivery intensity of HeLa cells treated in PBS, PBS+Ca (1.8mM Ca), PBS+Na (2.7mM Na), and PBS+EDTA (1.8mM EDTA) using a 50-6 device. **b)** Corresponding viability data as measured by propidium iodide staining. Mean intensity of cascade blue conjugated 3kDa dextran was measured by flow cytometry and normalized against the control to account for background effects (e.g. endocytosis and surface binding). Error bars represent 2 standard deviations among triplicates.

Note that the use of a chelating agent (EDTA) led to enhanced delivery and toxicity. Although it is difficult to rule-out the potential intracellular toxicity of EDTA, these results would be consistent with the notion that active chelation of Ca removes any trace amounts from the cell suspension and thus retards membrane repair more severely. The addition of an alternative cation (sodium) did not produce an effect similar to that of calcium. These data indicate that changes in the buffer's ion content (i.e. osmolarity) are probably not responsible for the observed effects.

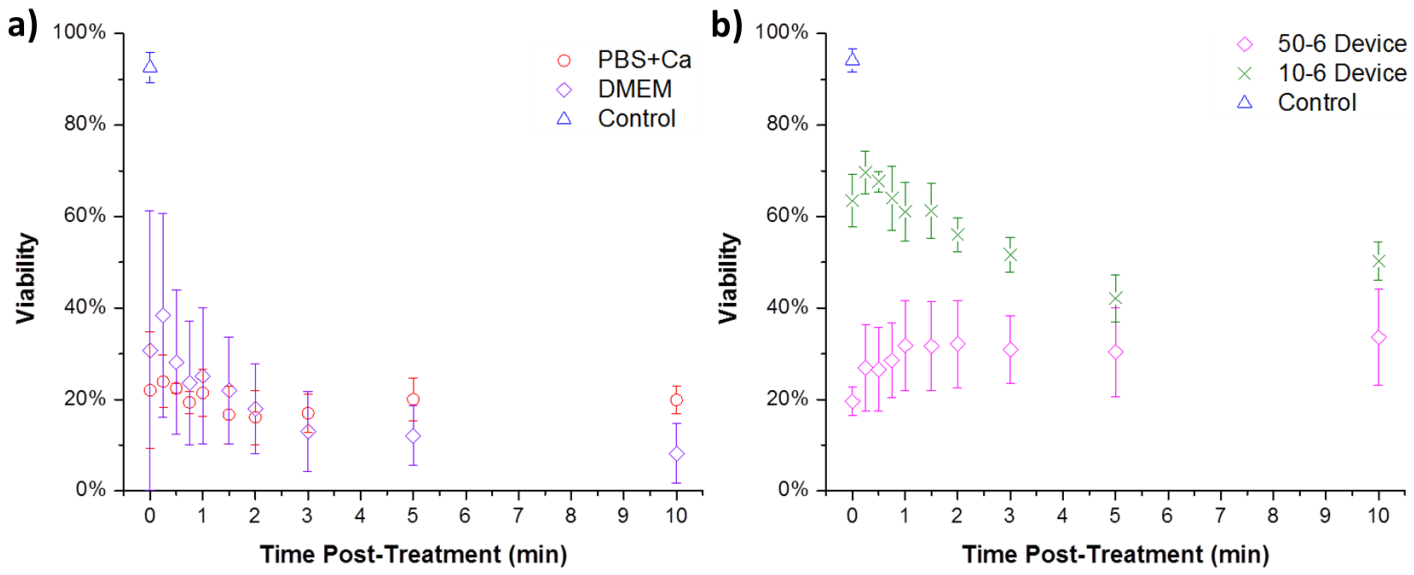

Figure S8. Viability data for membrane recovery experiments. These viability data correspond to the experiments shown in **Fig. 4**. Results were measured by flow cytometry and viability was measured by propidium iodide staining. Error bars represent 2 standard deviations among triplicates.

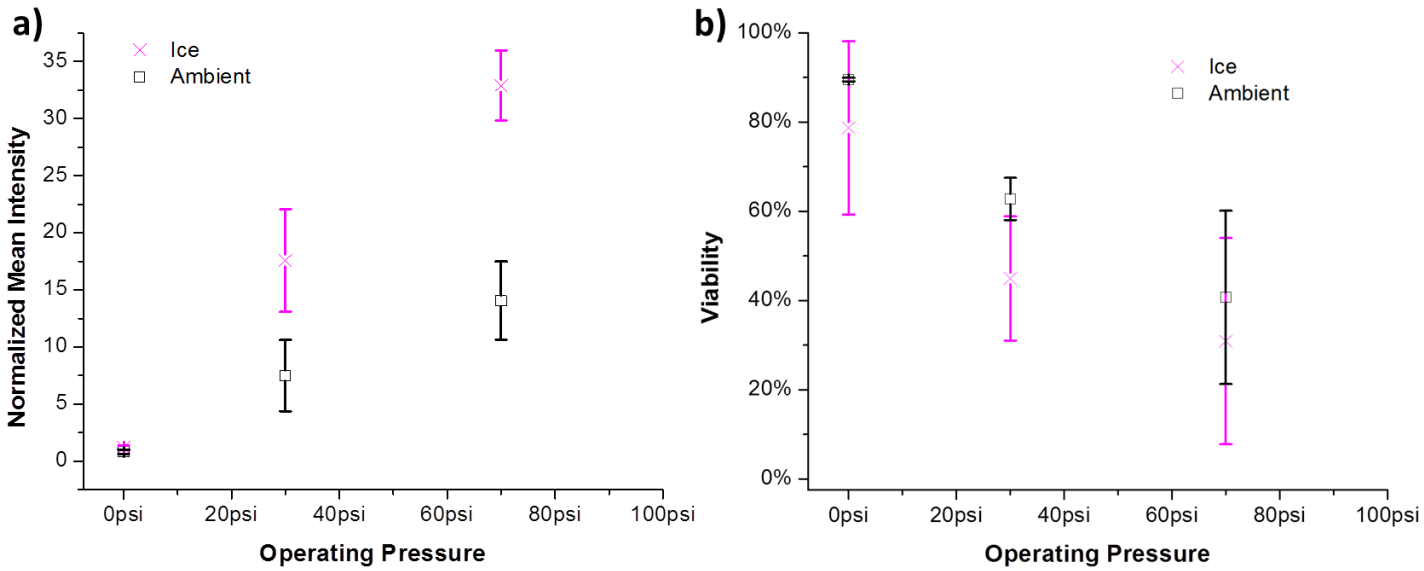

Figure S9. The influence of temperature on delivery efficiency. a) Normalized delivery intensity of HeLa cells treated in PBS using a 50-6 device. 'Ambient' cases were run as described earlier. For the 'ice' cases, the cell suspension+delivery material, the device setup, and collection plate were incubated on ice for 5min prior treatment. Treatment was conducted on ice and the cells were maintained on ice for >5min post-treatment. **b)** Corresponding viability data as measured by propidium iodide staining. Mean intensity of cascade blue conjugated 3kDa dextran was measured by flow cytometry and normalized against the control to account for background effects (e.g. endocytosis and surface binding). Error bars represent 2 standard deviations among triplicates.

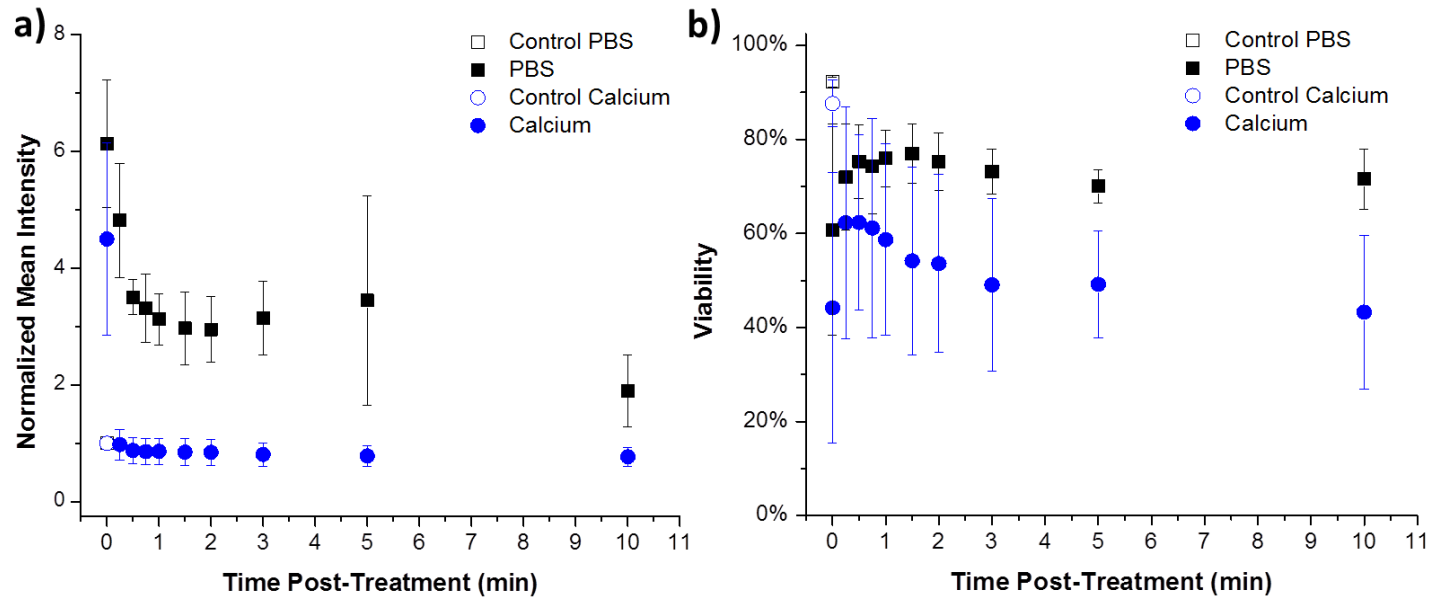

Figure S10. Pore closure kinetics are calcium dependent in T cells. a) Normalized intensity of naïve T cells treated in the absence of dyes and subsequently exposed to cascade blue conjugated 3kDa dextran

at the specified time points. PBS and PBS supplemented with 1.8mM of calcium were used as buffers during these experiments. The control cases correspond to cells that were exposed to dye but not treated by the device. **b)** The corresponding viability data for each treatment time. Mean intensity of cascade blue conjugated 3kDa dextran was measured by flow cytometry and normalized against the control to account for background effects (e.g. endocytosis and surface binding). Error bars represent 2 standard deviations among triplicates.

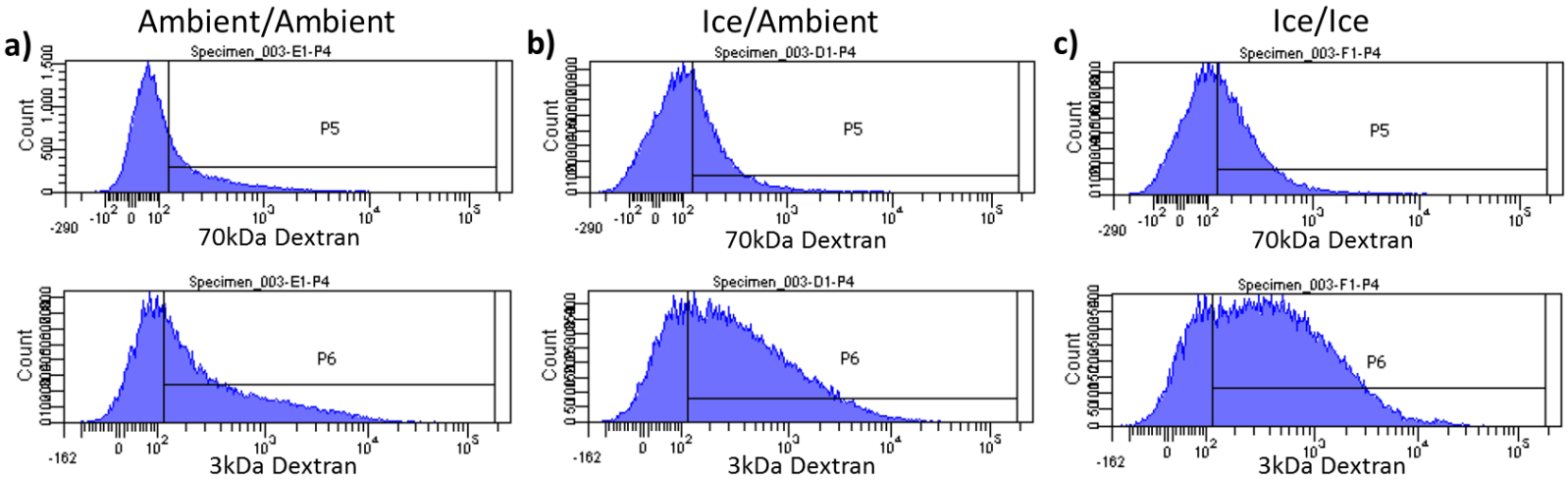

Figure S11. The influence of lower temperatures on delivery to T cells. Naïve murine T cells were treated under three different temperature conditions, in media, in the presence of cascade blue conjugated 3kDa dextran and fluorescein conjugated 70kDa dextran. **a)** Cells were treated by the device at ambient conditions and allowed to recover at ambient conditions for >5min post-treatment. **b)** Cells and the device were placed on ice for >2min prior to treatment. Treatment was conducted on ice and cells were allowed to recover at ambient conditions for >5min post-treatment. **c)** Cells and the device were placed on ice for >2min prior to treatment. Treatment was conducted on ice and cells were allowed to recover on ice for >5min post-treatment. Results were measured by flow cytometry and dead cells were excluded using propidium iodide staining.

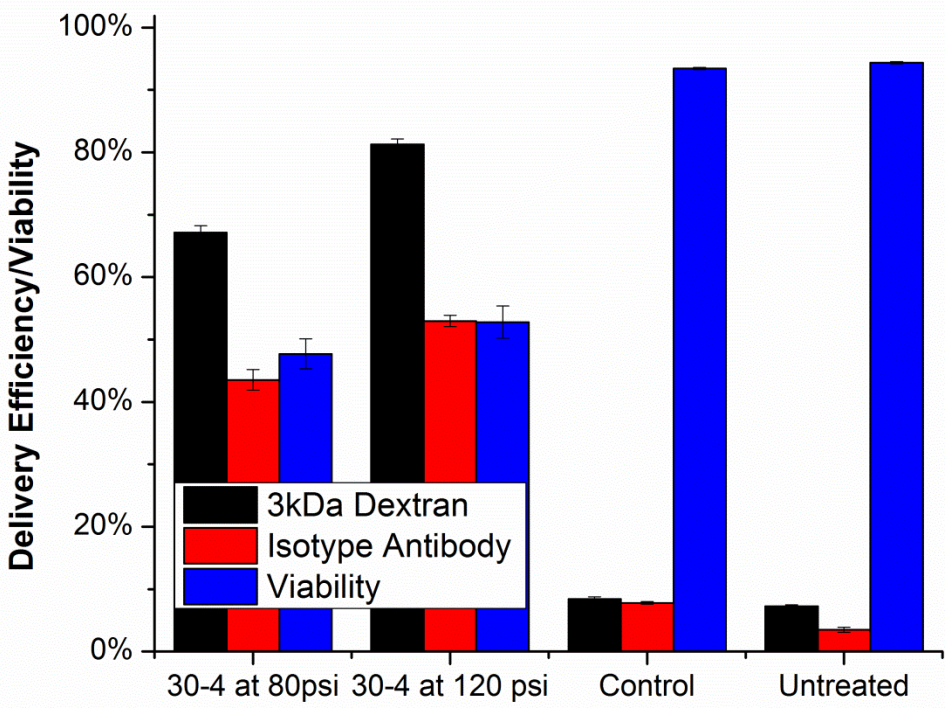

Figure S12. Intracellular delivery of dextran and antibodies to Naïve murine T cells. Naïve murine T cells were treated on ice (as described in **Fig. S11c**) in the presence of 3kDa Dextran and mouse IgG1 isotype control antibodies. Delivery efficiency and viability were measured by flow cytometry and propidium iodide staining. Control samples were exposed to the delivery material for at least the same amount of time as the device samples.